Magnetic properties of ferrofluid change over time: Implications for magnetic pore fabric studies

A.R. Biedermann[1], J.M. Parés[2]

[1]Institute of Geological Sciences, University of Bern, Bern, Switzerland

[2]CENIEH, Burgos, Spain

Corresponding author: Andrea R. Biedermann (andrea.biedermann@geo.unibe.ch)

Key Points:

- Changing ferrofluid properties, e.g. particle aggregation, affect impregnation process and magnetic pore fabric degree, shape or orientation
- Susceptibility of rock impregnated with oil-based fluid increases over time, affecting impregnation efficiency calculations
- Statements on impregnation efficiency of oil- vs water-based ferrofluids need to be re-evaluated

This article has been accepted for publication and undergone full peer review but has not been through the copyediting, typesetting, pagination and proofreading process, which may lead to differences between this version and the Version of Record. Please cite this article as doi: 10.1029/2022JB024587.

Abstract

The anisotropy of magnetic susceptibility of ferrofluid-impregnated samples is an efficient and powerful proxy for pore space anisotropy and preferred flow directions. One of the main assumptions in pore fabric studies is that all pores > 10-20 nm are homogeneously filled with ferrofluid, and that the ferrofluid has constant properties throughout the pore space and over time. If only part of the pore space is filled, this can lead to artefacts. Additionally, because magnetic anisotropy of a given pore space depends on fluid susceptibility, quantitative interpretations may be affected by the interval between impregnation and measurement time, or by the age of the ferrofluid during impregnation, unless fluid properties remain constant. A careful investigation of the time variation of ferrofluid properties and magnetic pore fabrics in synthetic and natural samples shows time-dependence of susceptibility and hysteresis properties, related to dissolution of particle surfactants, and deterioration of colloidal stability. The latter leads to particle aggregation and sedimentation, which changes the anisotropy properties, and also affects impregnation behaviour. Natural samples impregnated by oil-based ferrofluid also experience a 2.5- to 3-fold increase in mean susceptibility, with important consequences for the susceptibility-based determination of impregnation efficiency. Based on our results, we recommend that ferrofluid properties are determined at the time of impregnation, and that samples are measured shortly after impregnation.

Plain Language Summary

One way to describe a rock's pore space, i.e. properties relevant for the flow of groundwater or hydrocarbons, is to fill all pores with a strongly magnetic fluid and then measuring the magnetic properties and their directional dependence. This method is reliable if all pores are filled with the magnetic fluid, and the magnetic properties of the fluid are known. Challenges occur when the magnetic particles in the fluid cluster together and become too big to enter smaller pores, only part of the pores are filled with magnetic fluid, the magnetic fluid changes its properties over time, or the magnetic properties of the rock change upon contact with the fluid. These processes are investigated here, using both synthetic samples and rocks. We show that particles cluster and magnetic properties change over time, showing the need to re-evaluate some previous statements.

1 Introduction

Directional properties of pore space, including the preferred shape, alignment and connectivity of pores, control preferred flow directions in porous media. This pore fabric is thus an important input parameter for aquifer and reservoir modelling, to understand sub-surface flow patterns, and to predict fluid paths (Ayan et al., 1994; Bear, 2013; Bear, Braester, & Menier, 1987; Huang, Tao, Li, Lyu, & Guo, 2017; Ijeje, Gan, & Cai, 2019; Panja, McLennan, & Green, 2021; Rasolofosaon & Zinszner, 2002; Sinan, Glover, & Lorinczi, 2020; Storesletten, 1998; Wang, Huang, Lu, Tang, & Li, 2019; Willems, Nick, Donselaar, Weltje, & Bruhn, 2017).

Magnetic pore fabrics (MPFs) serve as a time-efficient and powerful proxy for pore fabrics and permeability anisotropy. They describe the 3D connected pore space without any a priori knowledge on pore fabric orientation. A wide range of pore sizes, potentially down to 10nm (Almqvist, Mainprice, Madonna, Burlini, & Hirt, 2011; Benson, Meredith, & Platzman, 2003; Louis et al., 2005; J. Parés, Miguens, & Saiz, 2016; Robion et al., 2014), is captured in a representative sample volume (~10 cm^3). All directional measurements are done on a single core unlike e.g. seismic or permeability anisotropy measurements that may be affected by between-sample heterogeneity. Magnetic anisotropy can be measured using a scheme of 15 directional (averaged) susceptibilities, or susceptibility differences in perpendicular planes (Biedermann, Lowrie, & Hirt, 2013; Jelinek, 1977, 1996), providing an extremely accurate measure of the anisotropy. Magnetic pore fabrics are determined by impregnating a rock with a high-susceptibility ferrofluid, and then measuring the anisotropy of its magnetic susceptibility. Empirical relationships exist between (1) the fabric orientation of MPFs and the shape preferred pore alignment (Pfleiderer & Halls, 1990, 1993); (2) the degree of MPF anisotropy and ratio of maximum to minimum pore axial length (Jones, Benson, & Meredith, 2006; Pfleiderer & Halls, 1990, 1993); and (3) the shape of the MPF ellipsoid and the pore shape (Jones et al., 2006). Note that the relationships between MPF anisotropy degree and pore axial ratio, and between anisotropy shape and pore shape are strictly valid for simple synthetic samples with only one single pore. Natural samples contain numerous pores, and therefore, the pore shape, axial ratio, shape preferred orientation, and distribution of pores together define the MPF anisotropy parameters (Biedermann, 2019, 2020). The concept of total shape ellipsoid has been introduced recently to obtain an integrated measure of shape and axial ratio of individual pores and their alignment in a rock, that can be compared directly to second order tensor properties (Zhou et al., in review). Further relationships exist between the orientation and degree of permeability anisotropy and MPF orientation and anisotropy degree (Hailwood, Bowen, Ding, Corbett, & Whattler, 1999; Nabawy, Rochette, & Géraud, 2009; Pfleiderer & Halls, 1994). As both MPF and permeability anisotropy are second order tensor properties, these quantities are in principle easier to compare. However, permeability is often not measured as a full tensor but rather along two or three directions parallel to the macroscopic fabric, resulting in uncertainty, and can additionally be affected by heterogeneity, leading to larger variability in empirical results.

Despite these promising empirical observations, some challenges arise when interpreting magnetic fabrics. First and most importantly, the empirical relationships are not always valid (Nabawy et al., 2009). This may be partly related to difficulties when comparing 2D and 3D data, resolution artefacts, measurements on single vs multiple cores, or changes to pore space during sample preparation. Another important aspect is that MPFs have been primarily related to the average pore shape (Hrouda, Hanak, & Terzijski, 2000; Pfleiderer & Halls, 1993), but the distribution of the pores and related interactions also lead to distribution anisotropy

(Biedermann, 2019, 2020; Jones et al., 2006). Further, cracks can largely affect the measured MPFs (Humbert et al., 2012; Pugnetti, Zhou, & Biedermann, 2022). Differences in magnetic susceptibilities of the used ferrofluids, and the frequency-dependence of ferrofluid susceptibility lead to further variability (Biedermann, 2019; Biedermann, Pugnetti, & Zhou, 2021; Jones et al., 2006). An additional challenge specific to MPFs is that the pore space may not be fully impregnated, e.g. ferrofluid not reaching the center (Almqvist et al., 2011), or being blocked by narrow pore throats (Robion et al., 2014). Complex pore shapes with high tortuosity (Clennell., 1997; Ghanbarian, Hunt, Ewing, & Sahimi, 2013) may further aggravate these issues. Potential solutions are smaller samples (J. Parés et al., 2016), or improved impregnation methods (Pugnetti et al., 2022). Finally, particle aggregation and sedimentation during or after impregnation may affect measured MPFs (Biedermann et al., 2021) by changing ferrofluid properties and creating particle distributions that no longer reflect the pore geometry.

Magnetic properties of nanoparticles and ferrofluid that contains nanoparticles vary largely with grain size, surfactants, and with dilution which defines magnetic between-particle interactions. In theory, the smallest grains are superparamagnetic (SP), with zero remanence and coercivity, and high susceptibility. As their size increases, they become stable single domain (SSD), and the coercivity and remanence increase while susceptibility decreases. As size increases further, a single domain is energetically no longer favourable, and the grain becomes multidomain (MD), with an associated decrease of remanence stability (Figure 1a) (Caizer, 2016; Clark, 1997; Dearing et al., 1996; Dunlop, 1981, 2002a; Eyre, 1997; Hrouda, 2011; Huber, 2005; Lee, Cha, Yoon, Lee, & Kim, 2015; Stephenson, 1971; Worm, 1998). The SP-SSD and SSD-MD transition sizes for magnetite depend on grain shape, and have been estimated to 20-30 nm and 50-130 nm, respectively (Clark, 1997; Day, Fuller, & Schmidt, 1977; Dunlop, 1981; Eyre, 1997; Li et al., 2017). The SP-SSD threshold depends on measurement time, and the 20-30 nm apply to coercivity and remanence measurements. Susceptibility can be measured in either DC or AC fields, and for AC measurements, the SP-SSD transition occurs at lower grain sizes at higher measurement frequencies (Figure 1b) (Dearing et al., 1996; Hrouda, 2011).

Nanoparticles are often described to have a core-shell structure, with an inner ferrimagnetically ordered magnetite core, and a shell in which spins are disordered due to surface effects, e.g., lower coordination numbers for surface spins. Therefore, the magnetic size of nanoparticles is generally smaller than their physical size. Furthermore, surfactants may influence the surface spins due to their bonds, resulting in large changes of magnetization when the same type of particle is coated with different surfactants; strongly interacting surfactants have larger effects on the nanoparticle magnetic properties, decreasing saturation magnetization, and increasing coercivity due to directional bonding that prevents spin reorientation (Berkowitz et al., 1999; Caizer, 2016; Caruntu, Caruntu, & O'Connor, 2007; Hiemstra, 2018; Huber, 2005; Muscas et al., 2013; Papaefthymiou, 2009; Smolensky et al., 2013; Söffge & Schmidbauer, 1981). Step-like magnetization changes in hysteresis curves were observed in some studies, and attributed to frustration and disorder of surface spins (Rani & Varma, 2015), or interactions (Trukhan, Martyanov, & Yudanov, 2011). While there is agreement that interactions between particles affect magnetic properties including magnetization and coercivity (Balaev et al., 2017; Caruntu et al., 2007; Dunlop, 2002a; Joseph & Mathew, 2014), both increases (Caruntu et al., 2007; Knobel et al., 2007; Nadeem et al., 2011) and decreases in coercivity (Trukhan et al., 2011) have been postulated as a result of increased interactions, potentially depending on bonding angles (Lu, Lin, Kuo, & Huang, 1999). Caruntu et al. (2007) observed that the relationships between concentration and magnetic properties are non-linear. Some particles form clusters, and act as a

single larger particle (Lee et al., 2015). Together, all these complexities result in a wide range of magnetic properties observed for particles of the same size (Figure 2) (Caizer, 2016; Caruntu et al., 2007; Day et al., 1977; Goya, Berquó, Fonseca, & Morales, 2003; Heider, Zitzelsberger, & Fabian, 1996; Iida, Takayanagi, Nakanishi, & Osaka, 2007; Johnson, Lowrie, & Kent, 1975; Lee et al., 2015; Li et al., 2017; Ma et al., 2004; Parry, 1965; Rani & Varma, 2015; Salazar et al., 2011; Smolensky et al., 2013; Upadhyay, Parekh, & Pandey, 2016; Xie et al., 2006).

Because of the many factors influencing nanoparticle magnetic properties and the importance of ferrofluid properties for the quantitative interpretation of MPFs, this study investigates how magnetic properties of nanoparticles in ferrofluids and related MPFs vary over time, and the sources of these variations. Both synthetic samples and natural silty sandstones are studied. Based on these results, we discuss how to best measure and interpret MPFs in terms of pore fabric and permeability anisotropy.

2 Materials and Methods

2.1 Time-dependent properties of synthetic samples

2.1.1 Sample preparation

Synthetic samples were prepared to investigate MPFs and potential variation over time on a simple and controlled system, with a single void of known geometry. Voids of 1 mm diameter and 2 mm depth were drilled into transparent polycarbonate cubes of a few mm side length, with an HSS/CNC drill (high speed steel, computerized numerical control) at the Institute of Geological Sciences, University of Bern. The sample *z*-axis was chosen along the cylinder axis, and *x* and *y* in the symmetry plane. The small size of the samples is essential, as we intended to measure hysteresis properties, and the vibrating sample magnetometer (VSM) is prone to artefacts related to a spatial variation in the instrument response function (Kelso, Tikoff, Jackson, & Sun, 2002). These geometrical effects are minimized when using small samples. Initially, one sample each was filled with water-based EMG304, EMG705, and with oil-based EMG901, EMG909, at a 1:10 concentration of ferrofluid to carrier liquid. The specified intrinsic initial susceptibilities of these fluids are 5.03, 4.04, 6.79, and 1.38 (SI), respectively (ferrofluid.ferrotec.com/products/ferrofluid-emg). After filling, the voids were sealed with diamagnetic hot glue, as this was the most stable seal over time according to Biedermann et al. (2021). At a later stage, eight additional samples were prepared using 1:5 and 1:20 concentrations of the same types, but a different batch of ferrofluids. First results indicated that the labels of the 1:5 and 1:20 concentrations of the EMG304 samples had been switched, and additional samples of EMG304 at these concentrations were prepared ~1 month later from the second batch of ferrofluid. In-between measurements, sample were stored with their *z*-axis vertical.

2.1.2 Expected MPF properties

From the ferrofluids' specified properties, fluid concentration, and void geometry, the expected directional susceptibilities, mean susceptibility and anisotropy parameters were calculated. Given the large fluid susceptibility, the shape of the void controls the measured anisotropy due to self-demagnetization, as long as the particles within the fluid are distributed evenly throughout the void. The self-demagnetization factors (N) for cylindrical shapes can be calculated based on the equations in Sato and Ishii (1989), giving $N_x = N_y = 0.409$, and $N_z =$

0.181. Directional susceptibilities (k_{dir}) are defined by the intrinsic initial susceptibility (k_{int}) and the self-demagnetization factors as $k_{dir} = k_{int} / (1 + N_{dir}*k_{int})$, where $dir = x, y, z$, and the mean susceptibility as $k_{mean} = (k_x+k_y+k_z)/3$. The susceptibility of the carrier liquid was neglected, as it is orders of magnitudes lower than that of the ferrofluid itself (Biedermann et al., 2021), so that the susceptibility of the diluted ferrofluid was calculated from its k_{int} and dilution. For all samples, k_z is expected to reflect the maximum principal susceptibility k_1, and $k_x=k_y$ ($=k_2=k_3$), due to sample symmetry. Directional susceptibilities k_x, k_y, and k_z are measured along the x, y, and z axes, respectively, and $k_1 \geq k_2 \geq k_3$ refer to the principal susceptibilities, i.e., the eigenvalues of the susceptibility tensor. The anisotropy shape, defined as $U = (2*k_2-k_1-k_3)/(k_1-k_3)$ equals -1, reflecting the rotationally prolate symmetry of the void. The degree of anisotropy, $P = k_1/k_3$ varies with fluid type and concentrations, as it increases nonlinearly with fluid susceptibility for a given void shape (Figure 3a, Table S1). As the void shape remains constant, no changes in MPF properties are expected over time, unless the magnetic properties of the fluid or the distribution of nanoparticles within the void change.

2.1.3 Susceptibility measurements

Directional susceptibilities of the plastic cubes with their ferrofluid-filled voids were measured in alternating and direct current (AC and DC) fields, to characterize any variability of the ferrofluid properties with measurement type. Note that the intrinsic fluid susceptibilities are specified as DC susceptibilities (ferrotec.com), whereas all MPF studies that specified the instruments used or type of measurement determined AC susceptibility and its anisotropy (Benson et al., 2003; Esteban, Géraud, & Bouchez, 2006; Hrouda et al., 2000; Humbert et al., 2012; Jones et al., 2006; Nabawy et al., 2009; J. Parés et al., 2016; Pfleiderer & Halls, 1990, 1993, 1994; Robion et al., 2014). Because differences have been reported in nanoparticle properties in DC vs AC fields (Goya et al., 2003), or with measurement frequency of the AC field (Biedermann et al., 2021), it is important to better understand how DC and AC susceptibilities of ferrofluids relate to one another.

AC susceptibility measurements were conducted at 200 A/m, and in up to three frequencies (976 Hz, 3904 Hz, and 15616 Hz) on an Agico MFK1-FA in the Laboratory of Natural Magnetism at ETH Zürich, Switzerland. Due to sample symmetry and to optimize measurement time, susceptibility was measured along three directions, x, y and z, rather than the full set of 15 directions that is used normally to define the full susceptibility tensor when nothing is known about a samples' anisotropy (Jelinek, 1977). Each directional measurement was repeated 3-5 times to improve and assess data quality. The first measurements were performed within the first days after sample preparation (once the glue had dried), and measurements were repeated for several months thereafter. The aim was to obtain a new dataset every month, but the timeline was affected by lockdowns and associated restricted access to university buildings. Therefore, the timesteps are irregular. Note that the ferrofluid manufacturer states that '[t]here is a tendency for magnetic particles to form aggregates in water-based ferrofluids. For best results, use within three months of purchase', while no similar statement is made for oil-based fluids. Therefore, a change in properties is expected for water-based fluids EMG304 and EMG705 after 3 months. Nevertheless, these results are included here to quantify the effect of aggregation within the first three months, and for older samples.

DC susceptibilities were extracted from initial magnetization curves, measured on a Princeton 3900 VSM. Multiple segments were used to ensure accurate data in weak fields: 0.5

mT steps and 200 ms averaging time for fields between 0 mT and 100 mT, and larger steps at higher fields. Initial magnetization curves were measured and analysed for up to three directions at each time step. However, because the asymmetry of the samples made measurements along *z* difficult, most initial magnetization curves were measured along *x*. Only the lowest fields were used to determine initial susceptibility k_{ini}, using raw or smoothed data depending on the noise level in the measurements. When noise level was low, k_{ini} was calculated directly as the slope of the raw magnetization (*M*) vs field (*H*) data, $k_{ini} = \Delta M / \Delta H$, and for higher noise levels, magnetization data was smoothed with a moving average filter prior to calculating the slope. The slope changes rapidly even in these weak fields, so that the obtained susceptibility depends on ΔH. To make these comparable, initial susceptibilities are shown as curves for fields between 0 and 20 mT.

2.1.4 Hysteresis and remanence curve measurements

Hysteresis parameters were extracted from multi-segment loops with maximum fields of ±500 mT. Note that not all samples are fully saturated in these fields, but larger fields were not possible due to relatively large pole spacing necessary to fit the asymmetric voids of the relatively large samples. Similar to DC susceptibility data, *x*, *y*, and *z* directions were measured initially, but mostly the *x*-direction for later measurements. Field increments of 5 mT were used in large fields (±200 mT to ±500 mT), 2 mT increments in intermediate fields (±100 mT to ±200 mT), and 0.5 mT increments in fields <±100 mT. Averaging times varied between 100 ms and 200 ms. Hysteresis data was processed with own Matlab codes, or using HystLab (Jackson & Solheid, 2010; Paterson, Zhao, Jackson, & Heslop, 2018).

Backfield remanence curves were obtained on the same instrument, obtaining 250 measurements with logarithmic field increments up to a maximum field of -500 mT. Remanence curves were mainly measured parallel to *x*, and not all samples could be measured right after preparation.

2.2 Time-dependent MPF of natural red sandstone

2.2.1 Sample preparation and initial characterization

J. Parés et al. (2016) measured MPFs of Lower Triassic red silty sandstones from the classic European Buntsandstein facies, in the Iberian Range (N Spain). These rocks were selected because their rock and paleomagnetic characteristics are well known (Dinarès-Turell, Díez, Rey, & Arnal, 2005; J. M. Parés & Dinarès-Turell, 1994; Rey, Turner, & Ramos, 1996; Turner, Turner, Ramos, & Sopeña, 1989), and they typically have a reasonably high porosity, partially due to open cleavage in mica grains. Porosity was determined on representative samples by mercury intrusion porosimetry with an Autopore IV (Micromeritics), and is 16 %. Pore size distribution analysis reveals that < 0.1 µm pores control up to 43 % of the volume porosity, which translates to a specific surface area of 3.84 m^2/g. The specimen size (height 17 mm, diameter 18 mm) was chosen such that they could be encapsulated into standard, non-magnetic, 7 cm^3 plastic boxes with rounded edges. Measuring these plastic boxes instead of the impregnated specimens minimizes ferrofluid contamination. As a consequence, the original MPF measurement procedure described elsewhere (Benson et al., 2003; Pfleiderer & Kissel, 1994; Robion et al., 2014) was modified by J. Parés et al. (2016) in that they used smaller, encapsulated specimens (~4 cm^3 as opposed to the standard 10 cm^3), and measured them with a highly sensitive bridge (Figure 3b,c).

AMS was measured on a MFK1-FA Kappabridge (AGICO Instruments), a fully automated inductive bridge, at a frequency of 976 Hz and a field of 200 A/m. Magnetic susceptibility was determined on a slowly spinning specimen (Jelinek, 1996), and the operator just needed to adjust the specimen in three perpendicular positions. This measurement takes ~2 minutes per specimen and is very precise, due to many susceptibility determinations in each plane perpendicular to the axis of specimen rotation. Data was processed using the Safyr software (AGICO, Czech Republic), which combines the measurements in three perpendicular planes plus one bulk value to compute a full susceptibility tensor, and measurement errors are determined based on multivariate statistics. High-temperature susceptibility curves and hysteresis loops were obtained on the MFK1-FA and a MicroMag 3900 vibrating sample magnetometer (VSM - Princeton Measurements Corporation), respectively, to identify the main magnetic carriers in these rocks.

2.2.2 MPFs and their time-variation

Samples were dried in a standard Memmert 200 oven for 24 hours at 40 °C, and their weight was measured prior to impregnation. Samples were impregnated in a Logitech IU30 vacuum chamber (J. Parés et al., 2016), using EMG905 ferrofluid (Ferrotec), consisting of superparamagnetic magnetite particles (nominal particle diameter of 10 nm; 7.8% by volume) in a light hydrocarbon oil, with an initial magnetic susceptibility of 3.5 SI. This was diluted with additional oil to a final concentration of 1 %, and a concomitant bulk susceptibility (1 ml) of 7.8 x 10^{-3} SI. Previous studies (e.g., Benson et al., 2003; Robion et al., 2014) revealed the effectiveness of this particular ferrofluid to impregnate geological samples, in particular compared to water-based ferrofluids. We prepared groups of eight specimens, which were placed in a glass beaker in the vacuum chamber and kept at a pressure of $4x10^{-2}$ mbar for 24 hours, after which injection with the ferrofluid solution started at $4x10^{-2}$ mbar. Specimens were placed in non-magnetic plastic boxes after drying for another 24 hours, to avoid contamination with the ferrofluid during subsequent handling. Weight was then remeasured, and subsequently MPFs were obtained with the MFK1-FA, using the same parameters as for the AMS measurement before impregnation. The bulk magnetic susceptibility of the impregnated samples is several times higher than that of the rock itself, and therefore the initial, natural rock magnetic susceptibility was neglected.

Measured specimens were stored in a refrigerator at a constant temperature of 5 °C. After about four years, MPFs were re-measured using the same instrumentation and software for data reduction. Samples were left at room temperature prior to repeat MPF measurements.

3 Results

3.1 Synthetic samples

3.1.1 Changes in AC and DC susceptibility over time

Susceptibility varies considerably over time, in particular for water-based fluids, with AC and DC susceptibilities as low as ~35 % of the value obtained at the same frequency right after sample preparation (k_0) (Figure 4a-f). The susceptibility of oil-based fluids was more stable (Figure 4g-m). None of the ferrofluids shows a clear and systematic behaviour at all concentrations, potentially related to the different batches of fluid used, or to concentration-dependent interaction effects. Therefore, the time-dependent behaviour is discussed for each

sample separately. The time-dependence of AC susceptibility will be discussed based on the evolution of k_{mean}, and that of DC susceptibility based on k_x.

For EMG304 at 1:5, the AC susceptibility for both samples was stable initially, followed by a pronounced decrease. The susceptibility of the first sample was 74-75 % of k_0 after 4-5 months, and varied between 36 – 38 % of k_0 during months 6-10 at 1 kHz. At 4 Hz (16 kHz), susceptibility had decreased to 82 % (86 %) and 41 – 44 % (44 – 48 %) of at an age of 5 or 6-10 months, respectively. The second sample showed a faster decrease during the first 4 months, to 62 % (69 %/75 %) at 1 kHz /4 kHz/16 kHz), and stabilized at 36 – 40 %, 42 – 45 %, and 46 – 51 % of k_0 thereafter. DC susceptibility increased during the first three months (104 – 122 % of k_0), followed by a decrease to 56 – 66 % of k_0 for the first, and 34 – 43 % k_0 for the second sample. At 1:10, the AC susceptibility decreases to 75 % of k_0 during the first month, and later on decreases further to 59 – 62 % of k_0 at 1 kHz. At 4 kHz (16 kHz), susceptibility decreases to 72 – 73 % (75 – 77 %) of k_0. DC susceptibility initially drops to 66 % k_0 (2.5 months), and then becomes stable at 81 – 89 % after 3.5 months. The most variable behaviour is observed at 1:20, where both AC and DC susceptibility decrease for the first sample, but show an initial increase to 113 – 119 % of k_0 for the second sample. AC susceptibility reaches 46 – 49 % / 52 – 56 % / 55 – 63 % and 49 – 52 % / 57 – 59 % / 61 – 65 % at 1 kHz / 4 kHz / 16 kHz for the first and second sample, respectively. DC susceptibility is 93 – 100 % and 52 – 54 % of k_0 for the first and second sample respectively. Interestingly, the sample with an initial increase in DC susceptibility reaches a lower susceptibility value after 6-10 months compared to the sample whose susceptibility decreased from the beginning.

For EMG705, the AC susceptibility at 1 kHz remains at 94 % of k_0 after one month at concentrations 1:5 and 1:20. Susceptibility stabilizes at 41 – 45 % (1 kHz), 48 – 50 % (4 kHz) and 55 – 59 % (16 kHz) of k_0 after 4 months. For concentration 1:10, susceptibility decreased slightly less, to 45 – 49 %, 52 – 55 % and 59 – 63 % at 1, 4 and 16 kHz, respectively. More variability was observed at 1:20 concentration, where the susceptibility at the 3 measurement frequencies decreased to 43 – 53 %, 46 – 58 %, and 51 – 67 %, respectively, 5 - 10 months after sample preparation. The DC susceptibility of EMG705 at concentration 1:5 increased to 104-108 % of the original value during the first two months, and ranged between 59 - 65 % of k_0 as the sample got older. A similar qualitative trend was displayed by the 1:20 concentration, with an initial increase to 112 % within the first 2 months, and a larger variability between 69 – 112 % thereafter. Conversely, the DC susceptibility of the 1:10 concentration dropped to 43 % after 2.5 months, followed by an increase to 65 – 78 % of k_0.

The AC susceptibility of EMG901 is relatively constant at 88 – 92 % of k_0 at 1:5, and 98 – 101 % of k_0 at 1:10, independent of measurement frequency. At 1:20, the susceptibility remains similar to the original value throughout the first month, and then decreases to 80 – 85 %. Conversely, the DC susceptibility shows an initial increase at both 1:5 (112 % after 4 months) and 1:20 (130 % after 2 months), followed by susceptibility decrease to 108 % and 85 – 102 % at 1:5 and 1:20, respectively. A different behaviour of DC susceptibility is observed for EMG901 at 1:10, with a drop to 60 – 63 % during the first months, reaching a maximum at 70 % of k_0 5.5 months after sample preparation, followed by another decrease to 63 %.

The AC susceptibility of EMG909 is relatively constant over time at all frequencies, and ranges between 93 – 97 %, 85 – 89 %, and 97 – 104 % of k_0 at 1:5, 1:10 and 1:20, respectively. The DC susceptibility shows a larger variation, with a drop to 89 % of k_0 after 1 month and 93 – 105 % after 2 - 10 months at 1:5. At 1:10, DC susceptibility displays a low of 71 % after 2.5

months, and remains at 78 – 80 % throughout the experiment. At 1:20, DC susceptibility varies randomly between 56 – 76 % of k_0.

A comparison between measured AC and DC susceptibility to the fluids' technical specifications shows that water-based EMG304 and EMG705 fluids exhibit susceptibilities significantly below the expected values, often far less than 50% (Figure 4a-f). The oil-based fluids EMG901 and EMG909 display susceptibilities larger than the expected value at 1:10, but lower than expected at 1:5 and 1:20, covering a total range of ~50 % to ~ 150 % (Figure 4g-m). This pattern is hard to explain with concentration dependence, and must be related to the use of fluids from different batches. Interestingly, the DC susceptibility of EMG901 at 1:10 gets close to the expected value 2.5 months after the sample was prepared.

To summarize, time variation in both AC and DC susceptibilities are most pronounced for water-based fluids. Especially for DC susceptibility, changes are largest in samples older than 3 months, as warned by the manufacturer, but they also occur within the first 3 months, both for AC and DC susceptibilities. Additionally, the water-based ferrofluids show a strong frequency-dependence, which becomes less as the samples age. Conversely, oil-based fluids have very little and constant frequency-dependence, but show differences between the samples prepared from different batches of ferrofluid.

3.1.2 Concentration-dependence of susceptibility

For non-interacting strongly magnetic particles in a non-magnetic carrier fluid, it is expected that the susceptibility increases with particle concentration. The AC susceptibilities of water and oil used to dilute the ferrofluids are $-1.0*10^{-5}$ and $-1.6*10^{-5}$ (SI), respectively, at ~1 kHz (Biedermann et al., 2021). Thus, their contribution to the susceptibility of the diluted ferrofluid is negligible. The diluted ferrofluid's susceptibility can be estimated as $k_{dil} = k_{ff} / (V_{ff} + V_{cl})$, where k_{dil} is the diluted susceptibility, k_{ff} the susceptibility of the pure ferrofluid, V_{ff} the volume of the pure ferrofluid, and V_{cl} the volume of additional carrier liquid.

The samples filled with EMG705 show the expected increase of AC and DC susceptibilities with ferrofluid concentration. An exception to this trend is the DC susceptibility after 2 months, which is lower at a ratio of ferrofluid to carrier liquid of 1:10 compared to 1:20. EMG304 follows the expected trend in some samples, but also shows the lowest susceptibility at 1:10 for several datasets. Note that the initial and repeat samples of EMG304 display different behaviour. Both oil-based fluids, EMG901 and EMG909 possess highest susceptibility at 1:10, and for older samples, the DC susceptibilities at 1:10 and 1:5 become comparable. No clear concentration-dependent trends are observed in the frequency-dependence of susceptibility (cf. Figure 4; Figure S1).

3.1.3 Anisotropy of AC susceptibility

The time-variation of the samples' anisotropy was assessed based on AC susceptibility, as DC susceptibility had been measured along only one direction at most time steps (Figure 5). From the sample geometry, it is expected that $k_z > k_x = k_y$, $U = -1$, and P varying with ferrofluid type and concentration. Measured anisotropies are highly variable, often showing k_z being smaller than the average of k_x and k_y, especially as time progressed. The anisotropy shape U changes from largely prolate to largely oblate during the experiment, with increasing anisotropy degree for the majority of samples (Figure 5a-i). The one exception is EMG909 with mostly

oblate anisotropy shapes at the start of the experiment, and more stable anisotropy degree over time (Figure 5k-m).

3.1.4 Hysteresis properties

Changes in hysteresis properties inform about potential changes to the particles, particularly their grain size and interactions. Saturation magnetization remains relatively constant throughout the duration of the experiment. Larger variability is observed for saturation remanence, coercivity and remanent coercivity (Figure 6, Figure S2). In theory, remanence and coercivity of SP particles are zero, and the measured values are low, which explains the noisy appearance of the data. Data variability between samples and time steps makes it challenging to identify clear and universal trends. However, there appears to be a slight increase over time for the saturation remanence and coercivity for EMG705 (Figure 6d) and to a lesser degree EMG304 (Figure 6a), whereas EMG909 exhibits decreasing saturation remanence and coercivity (Figure 6k). EMG901 shows a slight decrease in saturation remanence but almost no change in coercivity (Figure 6g). The remanent coercivity has a peak at ~2 months for the water-based fluids, before and after which it is very low. The oil-based fluids show an increase in remanent coercivity at 1:5 and 1:10 concentrations, but their behaviour at 1:20 is hard to interpret. Day plots are characterized by high B_{cr}/B_c and low M_r/M_s values. There is no clear grouping with respect to age or concentration of the samples. None of the data points coincide with the theoretical behaviour of 10 nm superparamagnetic magnetite (Day et al., 1977; Dunlop, 2002a, 2002b). Rather, the majority of measurements falls in the field commonly interpreted as multi-domain magnetite. However, the large B_{cr}/B_c ratios are typical for superparamagnetic grains.

Hysteresis loops and remanence curves display stronger changes over time for water-based fluids (EMG304 and EMG705; Figure 6c,f) compared to oil-based fluids (EMG901, EMG909; Figure 6i,m). One particularly interesting feature is the development of stepwise hysteresis in some of the EMG304 samples after 4-5 months. Note that all samples carry very weak remanences, thus resulting in noisy remanence curves, and related uncertainties in B_{cr}.

The concentration-dependence of M_s is similar to the concentration dependence of AC and DC susceptibility, with a clear increase of Ms with ferrofluid concentration for EMG705, larger variability for EMG304, and a peak of M_s at 1:10 for EMG901 and EMG909. The remaining properties show no clear concentration dependence, likely related to the fact that both M_r, B_c and B_{cr} are very weak and subjected to noise (Figure S3).

3.2 Rock magnetic properties and MPFs of natural rocks

Room-temperature hysteresis loops suggest a dominance of the paramagnetic over the ferromagnetic fraction in the dry specimens. After calculating the high-field susceptibility of the hysteresis loops, it is apparent that the paramagnetic fraction dominates the total magnetic susceptibility in dry samples. High-temperature susceptibility curves indicate that the ferromagnetic fraction is dominated by hematite. The magnetic fabric prior to impregnation essentially reflects preferred grain orientation of phyllosilicate minerals including both clays and mica grains, which make up to 4% of the total mineralogy of the Buntsandstein redbeds in this area (Marfil, La Iglesia, Herrero, Scherer, & Delgado, 2015). Minimum susceptibility axes are clustered around the pole to the bedding plane. Occasionally, the maximum axes are grouped, possibly indicating a paleocurrent direction (e.g., Tarling & Hrouda, 1993). Similar magnetic

fabric orientations have been observed in a vast majority of sedimentary rocks (J. M. Parés, 2015; Tarling & Hrouda, 1993), and reveal the deposition and further compaction of sediments.

A comparison between the MPF data measured after 4 years and the initial data described in J. Parés et al. (2016) indicates that the principal MPF axes remain almost identical to the initial MPFs, and the AMS of non-impregnated samples (Figure 7a). The coaxiality of the AMS and MPFs indicates that the orientation of the phyllosilicates controls the pore fabric of these rocks. The anisotropy degree (Pj) and shape (T) of the MPFs changed slightly after 4 years, but these changes are not statistically significant (Figure 7b,c). The anisotropy degree seems to decrease, and the anisotropy shape becomes less oblate. The main change is observed in the mean susceptibility (Figure 7d). After four years, all samples show a mean susceptibility that is 2.5 to 3 times higher than directly after impregnation.

4 Discussion

4.1 Stability of ferrofluid properties and MPF over time

Changes in MPF parameters over time can be caused by either of 2 processes, or a combination: (1) changes in ferrofluid magnetic properties over time, or (2) changes in the distribution of the particles within the void or pore (Figure 8). Changes in the ferrofluid magnetic properties may be associated with increased interactions between aggregated particles, or their collective behaviour as a larger particle, as observed in Lee et al. (2015). Another explanation for changes in magnetic properties could be that the coating of the particles changes over time. Because the coating affects the magnetic behaviour of nanoparticles (Berkowitz et al., 1999; Caizer, 2016; Caruntu et al., 2007; Hiemstra, 2018; Huber, 2005; Muscas et al., 2013; Papaefthymiou, 2009; Smolensky et al., 2013; Söffge & Schmidbauer, 1981), the fact that both EMG304 and EMG705 are coated with anionic surfactants while EMG901 and EMG909 have no coating, together with possible time-dependent changes in the coating likely explains the higher stability of the oil-based fluids over time. Importantly, while the largest changes in magnetic properties of water-based fluid occur after 4-5 months, changes to both susceptibility and hysteresis properties of the water-based fluids were observed also during the first three months, during which they were expected to be stable. Although the bulk magnetic properties of the oil-based fluids appear more stable over time, they seem more prone to aggregation and sedimentation of particles after short times, especially at a concentration of 1:20. Aggregation and sedimentation were also observed for oil-based fluids at 1:10 and 1:5, but at later time, and appeared slowest for the water-based fluids. These observations suggest that the coating of the water-based fluids initially protects them against aggregation, and magnetic properties change slightly while the coating slowly dissolves. Once a large part of the coating is dissolved, the particles aggregate, leading to more pronounced changes in their magnetic properties. Conversely, the oil-based fluids are less protected against aggregation as there is no coating, but because their surface spin structure is less affected by the presence or absence of coating, their magnetic properties are more stable (Figure 9).

A strong increase in AC and DC susceptibilities as well as saturation magnetization was observed for oil-based fluids at 1:10 compared to concentrations of 1:5 and 1:20, but not for water-based ferrofluids. There is no clear explanation for this behaviour, other than that the 1:10 samples had been prepared from a different batch of fluid than the 1:5 and 1:20 samples. Thus, the fluid may have had different properties or age upon the start of the experiment.

4.2 Rocks vs. synthetic samples

Two main differences were observed between rocks and synthetic samples. First, the fabric orientation, anisotropy degree and shape changes are relatively large in synthetic samples, but statistically significant changes between the initial MPF and the MPF after 4 years were not observed in the investigated rocks. Secondly, a pronounced increase in mean susceptibility occurred in rock samples, but not in the synthetic samples.

The fabric of the synthetic samples is markedly different from that of natural rocks. The former basically contain one single very large pore, whereas measurements on natural rocks integrate thousands of micropores and/or microcracks with different morphology. For the red siltstones investigated here, J. Parés et al. (2016) suggested that due to the size of the magnetite particles in the ferrofluid (10 nm), we need to seek the origin of the MPF in magnetite nanoparticles injected between clay flakes and between clays and other grains, facilitated by the platy nature of these minerals (cf Figure 3c). Hence, the MPF results in the natural rocks indicate that microporosity is controlled by clay fabrics, as the samples impregnated with ferrofluid mimic the magnetic fabric of the natural, dry samples. Thus, the nanoparticles can move freely in the relatively large pores of the synthetic samples, but are more constrained in natural rocks. Therefore, the nanoparticle distribution strongly differs between both types of samples, natural and synthetic, and might explain in part the differences we observe over time as well. Additionally, evaporation of the carrier liquid is expected to occur at different rates in both sample types, which may further explain the observed differences.

The changes in mean susceptibility over time that occur in natural rock cannot be explained by the evaporation of (diamagnetic) carrier liquid, as this would lead to a maximum susceptibility increase of $3*10^{-6}$ (SI). The observed increase on the order of 10^{-3} (SI) therefore has to be related to physical or chemical changes that happen due to the interaction between the ferrofluid and rock. The magnetite nanoparticles have a large surface area, and thus oxidation over time may be expected upon contact with air. However, the oxidation from magnetite to maghemite and hematite would decrease the susceptibility and cannot explain the observations. Water would preferentially leach Fe^{2+} from the magnetite particles, creating a more oxidized shell, and suppressing susceptibility due to lattice strain at the core-shell interface (van Velzen & Zijderveld, 1995). Dissolution of surfactant may influence the magnetic properties. Neither of these could explain the susceptibility increase for rocks impregnated with oil-based ferrofluids which have no coating. Particle aggregation is expected to cause a transition from SP to SD particles, thus decreasing susceptibility. Interestingly, empirical relationships exist between the presence of oil and strongly magnetic rocks. Abubakar et al. (2020) found a correlation between strongly magnetic samples and oil-stained samples, while unstained samples were more weakly magnetic. Mineral magnetic techniques have been used to identify hydrocarbon migration pathways and hydrocarbon contamination in soils and sediments (Badejo et al., 2021; Rijal, Porsch, Appel, & Kappler, 2012). Similarly, Gadirov, Eppelbaum, Kuderavets, Menshov, and Gadirov (2018) successfully identified hydrocarbon deposits from magnetic anomalies. From this, one could speculate that the oil reduced some of the hematite present in the samples to magnetite, as suggested by Abubakar et al. (2020). The observed susceptibility increase could be explained by formation of up to 0.1 vol.% magnetite, using the relationship between susceptibility and magnetite abundance from Clark (1997). However, Gendler et al. (2005) describe that reaction kinetics for transitions between iron oxides are slow at room temperature, and others report that microbial processes are crucial for such reactions at low temperatures

(Emmerton et al., 2013; Machel, 1995). Another possibility for the susceptibility increase is that the magnetite nanoparticles possessed an oxidized shell initially, with related lower susceptibility due to lattice strain (van Velzen & Zijderveld, 1995), and that this strain released over time, thus increasing susceptibility over the measurement period. While more work is needed to identify the process(es) causing the observed susceptibility increase, it is clear that the increase in mean susceptibility may have led to overestimating the impregnation efficiency of oil-based ferrofluid. This would have influenced previous statements that oil-based fluid is more efficient at impregnating rock than water-based fluid.

4.3 Recommendations for future MPF (and ferrofluid) studies

Ferrofluid properties, including their susceptibility, and hysteresis properties change over time, also within the 3-month period during which they are expected to be stable. Changes in magnetic properties reflect changes in the particles themselves, e.g. chemical alteration, dissolution of the surfactant of the particles in the water-based fluid, or particle aggregation. Because the fluid susceptibility affects the measured MPF, and particle aggregation prevents the ferrofluid from impregnating smaller pores, we recommend that fluid properties are monitored prior to impregnation and over time until the MPF measurements are completed. This is particularly important in studies that intend to interpret MPF anisotropy degrees quantitatively, or when assessing impregnation efficiency based on the change of susceptibility before and after impregnation.

Given the "rapidness" of particle aggregation, and potential sedimentation in larger pores, we consider it best to perform measurements "quickly" after impregnation. Nevertheless, as shown by the natural samples, the orientation of the MPF fabric and the anisotropy parameters were virtually the same several years after the initial measurements, likely due to particles not being able to move inside the small pores of these samples. Yet, because one does not know beforehand the pore structure or permeability, it is preferable to carry out MPF measurements right after the impregnation process.

We have observed significant changes to the mean susceptibility of natural redbed silty sandstones, although samples were kept refrigerated between initial and repeat measurements. At this point, it is not clear whether this change happened at constant rate over the 4-year timespan, or if a fast initial increase in mean susceptibility was followed by a slower change or constant susceptibility. If these changes occur fast after impregnation, this may result in overestimating the impregnation efficiency of oil-based ferrofluid, which in turn results in recommendations to prefer oil-based ferrofluid compared to water-based ferrofluid when aiming at high impregnation efficiency. Therefore, potential mineralogical changes that occur due to rock-fluiid interactions after impregnation need to be taken into account when estimating impregnation efficiency, both for water- and oil-based ferrofluid. While several studies have suggested that oil migration pathways or contamination can be tracked using magnetic methods, we are not aware of any study investigating the magnetic signature of the rock-oil interaction over time. Thus, more work will be needed to investigate the time-variation of magnetic properties as rock is in contact and reacts with oil, or oil-based ferrofluid, and the potential influence of mineralogy on these reactions.

The stability of the ferrofluid magnetic properties over time is only one aspect that helps determine which fluid is most suitable for a given study. Also the mineralogy of the investigated rocks is important, e.g., whether the constituent minerals are oil- or water-wetting (Abdallah et

al., 2007), or the effective porosity, pore size, and tortuosity of pores may play a role. Smaller and more tortuous pores have a higher need for a low-viscosity fluid with small molecules and particles, while larger pores are more easily impregnated also by higher-viscosity fluid. Additionally, the intended application will be important; groundwater flow will be best reflected by water-based ferrofluid, while hydrocarbon migration by oil-based ferrofluid. Thus, the fluid chosen to measure MPFs should be as close as possible to the fluid whose migration through the pore space is of interest. Finally, the choice of ferrofluid may be limited by the available impregnation methods, as water-based fluids boil off under vacuum conditions at room temperature, unless the vacuum can be controlled, and resin-based impregnation methods only work with oil-based fluids (Pugnetti et al., 2022).

5 Conclusions

The magnetic pore fabrics method is an efficient and powerful tool to investigate the shape, orientation and arrangement of pores in rocks. Their quantitative interpretation depends on the magnetic properties of the ferrofluid used to impregnate the pore space, and high impregnation efficiency is a prerequisite for reliable and robust interpretation.

Here, we have shown that ferrofluid magnetic properties change over time, and, additionally, interaction between ferrofluid and rock can lead to changes in mean susceptibility, with important consequences for the estimation of impregnation efficiency, and MPF interpretation. Moreover, particle aggregation and sedimentation in large pores may cause changes in the MPF, and effect that was not observed for natural samples with micropores. In any case, we recommend to characterize MPFs and impregnation efficiency within a day after impregnation.

Our results suggest that it is worth to reconsider earlier statements that oil-based fluids are more efficient at impregnating rocks compared to water-based fluids. Susceptibility increase due to mineralogical changes induced by oil-based fluid, and a susceptibility that is slightly above that stated in the fluid's technical specifications for oil-based fluid – compared to a susceptibility significantly below that in the technical specifications for water-based fluid – are factors suggesting that some of the conclusions in previous studies might need to be re-evaluated in the view of our findings.

Acknowledgments

Sandro Bula and Thomas Siegenthaler, Institute of Geological Sciences, University of Bern are thanked for preparing the synthetic samples, and Carlos Saiz, CENIEH, for thin section preparation. Constructive comments by Mark Dekkers, Bjarne Almqvist and two anonymous reviewers helped to improve the manuscript. We are grateful to the Department of Earth Sciences, ETH Zürich, for access to the Laboratory of Natural Magnetism. This project was funded by the Swiss National Science Foundation, project 176917, to ARB.

Open Research

Data is available at Zenodo: https://doi.org/10.5281/zenodo.6447563

References

Abdallah, W., Buckley, J. S., Carnegie, A., Edwards, J., Herold, B., Fordham, E., . . . Ziauddin, M. (2007). Fundamentals of Wettability. *Oilfield Review, 19*(2), 44-61.

Abubakar, R., Muxworthy, A. R., Fraser, A., Sephton, M. A., Watson, J. S., Heslop, D., . . . Southern, P. (2020). Mapping hydrocarbon charge-points in the Wessex Basin using seismic, geochemistry and mineral magnetics. *Marine and Petroleum Geology, 111*, 510-528. doi:10.1016/j.marpetgeo.2019.08.042

Almqvist, B. S. G., Mainprice, D., Madonna, C., Burlini, L., & Hirt, A. M. (2011). Application of differential effective medium, magnetic pore fabric analysis, and X-ray microtomography to calculate elastic properties of porous and anisotropic rock aggregates. *Journal of Geophysical Research-Solid Earth, 116*. doi:10.1029/2010jb007750

Ayan, C., Colley, G., Ezekwe, E., Wannell, M., Goode, P., Halford, F., . . . Pop, J. (1994). Measuring permeability anisotropy: The latest approach. *Oilfield Review, 6*, 24-35.

Badejo, S. A., Muxworthy, A. R., Fraser, A., Neumaier, M., Perkins, J. R., Stevenson, G. R., & Davey, R. (2021). Using magnetic techniques to calibrate hydrocarbon migration in petroleum systems modelling: A Case Study from the Lower Tertiary, UK Central North Sea. *Geophysical Journal International*. doi:10.1093/gji/ggab236

Balaev, D. A., Semenov, S. V., Dubrovskiy, A. A., Yakushkin, S. S., Kirillov, V. L., & Martyanov, O. N. (2017). Superparamagnetic blocking of an ensemble of magnetite nanoparticles upon interparticle interactions. *Journal of Magnetism and Magnetic Materials, 440*, 199-202. doi:10.1016/j.jmmm.2016.12.046

Bear, J. (2013). *Dynamics of Fluids in Porous Media*. New York, USA: Dover Publications Inc.

Bear, J., Braester, C., & Menier, P. C. (1987). Effective and relative permeabilities of anisotropic porous media. *Transport in Porous Media, 2*(3), 301-316.

Benson, P. M., Meredith, P. G., & Platzman, E. S. (2003). Relating pore fabric geometry to acoustic and permeability anisotropy in Crab Orchard Sandstone: A laboratory study using magnetic ferrofluid. *Geophysical Research Letters, 30*(19), 1976.

Berkowitz, A. E., Kodama, R. H., Makhlouf, S. A., Parker, F. T., Spada, F. E., McNiff Jr., E. J., & Foner, S. (1999). Anomalous properties of magnetic nanoparticles. *Journal of Magnetism and Magnetic Materials, 196-197*, 591-594.

Biedermann, A. R. (2019). Magnetic pore fabrics: the role of shape and distribution anisotropy in defining the magnetic anisotropy of ferrofluid-impregnated samples. *Geochemistry, Geophysics, Geosystems, 20*(12), 5650-5666. doi:10.1029/2019gc008563

Biedermann, A. R. (2020). FinIrrSDA: A 3D model for magnetic shape and distribution anisotropy of finite irregular arrangements of particles with different sizes, geometries, and orientations. *Journal of Geophysical Research: Solid Earth*, e2020JB020300. doi:10.1029/2020JB020300

Biedermann, A. R., Lowrie, W., & Hirt, A. M. (2013). A method for improving the measurement of low-field magnetic susceptibility anisotropy in weak samples. *Journal of Applied Geophysics, 88*, 122-130. doi:10.1016/j.jappgeo.2012.10.008

Biedermann, A. R., Pugnetti, M., & Zhou, Y. (2021). Explaining the large variability in empirical relationships between magnetic pore fabrics and pore space properties. *Geophysical Journal International, 227*(1), 496-517. doi:10.1093/gji/ggab230

Caizer, C. (2016). Nanoparticle Size Effect on Some Magnetic Properties. In *Handbook of Nanoparticles* (pp. 475-519).

Caruntu, D., Caruntu, G., & O'Connor, C. J. (2007). Magnetic properties of variable-sized Fe_3O_4 nanoparticles synthesized from non-aqueous homogeneous solutions of polyols. *Journal of Physics D: Applied Physics, 40*(19), 5801-5809. doi:10.1088/0022-3727/40/19/001

Clark, D. A. (1997). Magnetic petrophysics and magnetic petrology: aids to geological interpretation of magnetic surveys. *Journal of Australian Geology and Geophysics, 17*, 83-103.

Clennell., M. B. (1997). Tortuosity: a guide through the maze. In M. A. Lovell & P. K. Harvey (Eds.), *Developments in Petrophysics* (Vol. 122, pp. 299-344). London, UK: Geological Society, Special Publication.

Day, R., Fuller, M., & Schmidt, V. A. (1977). Hysteresis properties of titanomagnetites: grain-size and compositional dependence. *Physics of the Earth and Planetary Interiors, 13*, 260-267.

Dearing, J. A., Dann, R. J. L., Hay, K., Lees, J. A., Loveland, P. J., Maher, B. A., & O'Grady, K. (1996). Frequency-dependent susceptibility measurements of environmental materials. *Geophysical Journal International, 124*, 228-240.

Dinarès-Turell, J., Díez, B. J., Rey, D., & Arnal, I. (2005). "Buntsandstein" magnetostratigraphy and biostratigraphic reappraisal from eastern Iberia: early and middle triassic stage boundary definitions through correlation to Tethyan sections. *Palaeogeography, Palaeoclimatology, Palaeoecology, 229*, 158-177.

Dunlop, D. J. (1981). The rock magnetism of fine particles. *Physics of the Earth and Planetary Interiors, 26*, 1-26.

Dunlop, D. J. (2002a). Theory and application of the Day plot (Mrs/Ms versus Hcr/Hc) 1. Theoretical curves and tests using titanomagnetite data. *Journal of Geophysical Research, 107*(B3). doi:10.1029/2001jb000486

Dunlop, D. J. (2002b). Theory and application of the Day plot (Mrs/Ms versus Hcr/Hc) 2. Application to data for rocks, sediments, and soils. *Journal of Geophysical Research, 107*(B3). doi:10.1029/2001jb000487

Emmerton, S., Muxworthy, A. R., Sephton, M. A., Aldana, M., Costanzo-Alvarez, V., Bayona, G., & Williams, W. (2013). Correlating biodegradation to magnetization in oil bearing sedimentary rocks. *Geochimica et Cosmochimica Acta, 112*, 146-165. doi:10.1016/j.gca.2013.03.008

Esteban, L., Géraud, Y., & Bouchez, J. L. (2006). Pore network geometry in low permeability argillites from magnetic fabric data and oriented mercury injections. *Geophysical Research Letters, 33*, L18311. doi:10.1029/2006GL026908

Eyre, J. K. (1997). Frequency dependence of magnetic susceptibility for populations of single-domain grains. *Geophysical Journal International, 129*, 209-211.

Gadirov, V. G., Eppelbaum, L. V., Kuderavets, R. S., Menshov, O. I., & Gadirov, K. V. (2018). Indicative features of local magnetic anomalies from hydrocarbon deposits: examples from Azerbaijan and Ukraine. *Acta Geophysica, 66*(6), 1463-1483. doi:10.1007/s11600-018-0224-0

Gendler, T. S., Shcherbakov, V. P., Dekkers, M. J., Gapeev, A. K., Gribov, S. K., & McClelland, E. (2005). The lepidocrocite-maghemite-haematite reaction chain - I. Acquisition of chemical remanent magnetization by maghemite, its magnetic properties and thermal stability. *Geophysical Journal International, 160*(3), 815-832. doi:10.1111/j.1365-246X.2005.02550.x

Ghanbarian, B., Hunt, A. G., Ewing, R. P., & Sahimi, M. (2013). Tortuosity in porous media: a critical review. *Soil Science Society of America Journal, 77*(5), 1461-1477. doi:10.2136/sssaj2012.0435

Goya, G. F., Berquó, T. S., Fonseca, F. C., & Morales, M. P. (2003). Static and dynamic magnetic properties of spherical magnetite nanoparticles. *Journal of Applied Physics, 94*(5), 3520-3528. doi:10.1063/1.1599959

Hailwood, E. A., Bowen, D., Ding, F., Corbett, P. W. M., & Whattler, P. (1999). Characterizing pore fabrics in sediments by anisotropy of magnetic susceptibility analyses. In D. H. Tarling & P. Turner (Eds.), *Paleomagnetism and Diagenesis in Sediments* (Vol. 151, pp. 125-126): Geological Society, London, Special Publications.

Heider, F., Zitzelsberger, A., & Fabian, K. (1996). Magnetic susceptibility and remanent coercive force in grown magnetite crystals from 0.1 μm to 6 mm. *Physics of the Earth and Planetary Interiors, 93*, 239-256.

Hiemstra, T. (2018). Surface structure controlling nanoparticle behavior: magnetism of ferrihydrite, magnetite, and maghemite. *Environmental Science: Nano, 5*(3), 752-764. doi:10.1039/c7en01060e

Hrouda, F. (2011). Models of frequency-dependent susceptibility of rocks and soils revisited and broadened. *Geophysical Journal International, 187*(3), 1259-1269. doi:10.1111/j.1365-246X.2011.05227.x

Hrouda, F., Hanak, J., & Terzijski, I. (2000). The magnetic and pore fabrics of extruded and pressed ceramic models. *Geophysical Journal International, 142*, 941-947.

Huang, T., Tao, Z., Li, E., Lyu, Q., & Guo, X. (2017). Effect of permeability anisotropy on the production of multi-scale shale gas reservoirs. *Energies, 10*. doi:10.3390/en10101549

Huber, D. L. (2005). Synthesis, properties, and applications of iron nanoparticles. *Small, 1*(5), 482-501. doi:10.1002/smll.200500006

Humbert, F., Robion, P., Louis, L., Bartier, D., Ledésert, B., & Song, S.-R. (2012). Magnetic inference of in situ open microcracks in sandstone samples from the Taiwan Chelungpu Fault Drilling Project (TCDP). *Journal of Asian Earth Sciences, 45*, 179-189. doi:10.1016/j.jseaes.2011.10.009

Iida, H., Takayanagi, K., Nakanishi, T., & Osaka, T. (2007). Synthesis of Fe_3O_4 nanoparticles with various sizes and magnetic properties by controlled hydrolysis. *Journal of Colloid and Interface Science, 314*(1), 274-280. doi:10.1016/j.jcis.2007.05.047

Ijeje, J. J., Gan, Q., & Cai, J. (2019). Influence of permeability anisotropy on heat transfer and permeability evolution in geothermal reservoir. *Advances in Geo-Energy Research, 3*(1), 43-51. doi:10.26804/ager.2019.01.03

Jackson, M., & Solheid, P. (2010). On the quantitative analysis and evaluation of magnetic hysteresis data. *Geochemistry, Geophysics, Geosystems, 11*(4). doi:10.1029/2009gc002932

718 Jelinek, V. (1977). The statistical theory of measuring anisotropy of magnetic susceptibility of rocks and its
719 application.
720 Jelinek, V. (1996). Measuring anisotropy of magnetic susceptibility on a slowly spinning specimen - basic theory.
721 *AGICO Print No. 10*.
722 Johnson, H. P., Lowrie, W., & Kent, D. V. (1975). Stability of anhysteretic remanent magnetization in fine and
723 coarse magnetite and maghemite particles. *Geophysical Journal of the Royal Astronomical Society, 41*, 1-
724 10.
725 Jones, S., Benson, P., & Meredith, P. (2006). Pore fabric anisotropy: testing the equivalent pore concept using
726 magnetic measurements on synthetic voids of known geometry. *Geophysical Journal International, 166*,
727 485-492.
728 Joseph, A., & Mathew, S. (2014). Ferrofluids: synthetic strategies, stabilization, physicochemical features,
729 characterization, and applications. *ChemPlusChem, 79*(10), 1382-1420. doi:10.1002/cplu.201402202
730 Kelso, P. R., Tikoff, B., Jackson, M., & Sun, W. (2002). A new method for the separation of paramagnetic and
731 ferromagnetic susceptibility anisotropy using low field and high field methods. *Geophysical Journal*
732 *International, 151*(2), 345-359. doi:10.1046/j.1365-246X.2002.01732.x
733 Knobel, M., Nunes, W. C., Winnischofer, H., Rocha, T. C. R., Socolovsky, L. M., Mayorga, C. L., & Zanchet, D.
734 (2007). Effects of magnetic interparticle coupling on the blocking temperature of ferromagnetic
735 nanoparticle arrays. *Journal of Non-Crystalline Solids, 353*(8-10), 743-747.
736 doi:10.1016/j.jnoncrysol.2006.12.037
737 Lee, J. S., Cha, J. M., Yoon, H. Y., Lee, J.-K., & Kim, Y. K. (2015). Magnetic multi-granule nanoclusters: A model
738 system that exhibits universal size effect of magnetic coercivity. *Sci Rep, 5*, 12135. doi:10.1038/srep12135
739 Li, Q., Kartikowati, C. W., Horie, S., Ogi, T., Iwaki, T., & Okuyama, K. (2017). Correlation between particle
740 size/domain structure and magnetic properties of highly crystalline Fe3O4 nanoparticles. *Scientific Reports,*
741 *7*(1), 9894. doi:10.1038/s41598-017-09897-5
742 Louis, L., David, C., Metz, V., Robion, P., Menendez, B., & Kissel, C. (2005). Microstructural control on the
743 anisotropy of elastic and transport properties in undeformed sandstones. *International Journal of Rock*
744 *Mechanics and Mining Sciences, 42*, 911-923.
745 Lu, J. J., Lin, M. T., Kuo, C. C., & Huang, H. L. (1999). Hysteretic behavior of magnetic particles with dipole
746 interaction. *Journal of Applied Physics, 85*(8), 5558-5560. doi:10.1063/1.369894
747 Ma, M., Wu, Y., Zhou, J., Sun, Y., Zhang, Y., & Gu, N. (2004). Size dependence of specific power absorption of
748 Fe_3O_4 particles in AC magnetic field. *Journal of Magnetism and Magnetic Materials, 268*(1-2), 33-39.
749 doi:10.1016/s0304-8853(03)00426-8
750 Machel, H. G. (1995). Magnetic mineral assemblages and magnetic contrasts in diagenetic environments - with
751 implications for studies of palaeomagnetism, hydrocarbon migration and exploration. In P. Turner & A.
752 Turner (Eds.), *Palaeomagnetic Applications in Hydrocarbon Exploration and Production* (Vol. 98, pp. 9-
753 29). London, UK: Geological Society Special Publication.
754 Marfil, R., La Iglesia, A., Herrero, M. J., Scherer, M., & Delgado, A. (2015). Clay mineral occurrence and burial
755 transformations: reservoir potential of the Permo-Triassic sediments of the Iberian Range. *Basin Research,*
756 *27*(3), 295-309. doi:10.1111/bre.12074
757 Muscas, G., Concas, G., Cannas, C., Musinu, A., Ardu, A., Orrù, F., . . . Peddis, D. (2013). Magnetic Properties of
758 Small Magnetite Nanocrystals. *The Journal of Physical Chemistry C, 117*(44), 23378-23384.
759 doi:10.1021/jp407863s
760 Nabawy, B. S., Rochette, P., & Géraud, Y. (2009). Petrophysical and magnetic pore network anisotropy of some
761 cretaceous sandstone from Tushka Basin, Egypt. *Geophysical Journal International, 177*, 43-61.
762 Nadeem, K., Krenn, H., Traussnig, T., Würschum, R., Szabó, D. V., & Letofsky-Papst, I. (2011). Effect of dipolar
763 and exchange interactions on magnetic blocking of maghemite nanoparticles. *Journal of Magnetism and*
764 *Magnetic Materials, 323*(15), 1998-2004. doi:10.1016/j.jmmm.2011.02.041
765 Panja, P., McLennan, J., & Green, S. (2021). Influence of permeability anisotropy and layering on geothermal
766 battery energy storage. *Geothermics, 90*. doi:10.1016/j.geothermics.2020.101998
767 Papaefthymiou, G. C. (2009). Nanoparticle magnetism. *Nano Today, 4*(5), 438-447.
768 doi:10.1016/j.nantod.2009.08.006
769 Parés, J., Miguens, L., & Saiz, C. (2016). Characterizing pore fabric in sandstones with magnetic anisotropy
770 methods: initial results. *Journal of Petroleum Science and Engineering, 143*, 113-120.
771 doi:10.1016/j.petrol.2016.02.028
772 Parés, J. M. (2015). Sixty years of anisotropy of magnetic susceptibility in deformed sedimentary rocks. *Frontiers in*
773 *Earth Science, 3*. doi:10.3389/feart.2015.00004

Parés, J. M., & Dinarès-Turell, J. (1994). IberianTriassic paleomagnetism revisited: Intraplate block rotations versus polar wandering. *Geophysical Research Letters, 21*, 2155-2158.

Parry, L. G. (1965). Magnetic properties of dispersed magnetite powders. *The Philosophical Magazine: A Journal of Theoretical Experimental and Applied Physics, 11*(110), 303-312. doi:10.1080/14786436508221858

Paterson, G. A., Zhao, X., Jackson, M., & Heslop, D. (2018). Measuring, Processing, and Analyzing Hysteresis Data. *Geochemistry, Geophysics, Geosystems, 19*(7), 1925-1945. doi:10.1029/2018gc007620

Pfleiderer, S., & Halls, H. C. (1990). Magnetic susceptibility anisotropy of rocks saturated with ferrofluid: a new method to study pore fabric? *Physics of the Earth and Planetary Interiors, 65*, 158-164.

Pfleiderer, S., & Halls, H. C. (1993). Magnetic pore fabric analysis: Verification through image autocorrelation. *Journal of Geophysical Research, 98*(B3), 4311-4316.

Pfleiderer, S., & Halls, H. C. (1994). Magnetic pore fabric analysis: a rapid method for estimating permeability anisotropy. *Geophysical Journal International, 116*, 39-45.

Pfleiderer, S., & Kissel, C. (1994). Variation of pore fabric across a fold-thrust structure. *Geophysical Research Letters, 21*(19), 2147-2150.

Pugnetti, M., Zhou, Y., & Biedermann, A. R. (2022). Ferrofluid impregnation efficiency and its spatial variability in natural and synthetic porous media: Implications for magnetic pore fabric studies. *Transport in Porous Media*. doi:10.1007/s11242-022-01809-0

Rani, S., & Varma, G. D. (2015). Superparamagnetism and metamagnetic transition in Fe_3O_4 nanoparticles synthesized via co-precipitation method at different pH. *Physica B: Condensed Matter, 472*, 66-77. doi:10.1016/j.physb.2015.05.016

Rasolofosaon, P. N. J., & Zinszner, B. E. (2002). Comparison between permeability anisotropy and elasticity anisotropy of reservoir rocks. *Geophysics, 67*, 230-240.

Rey, D., Turner, P., & Ramos, A. (1996). Palaeomagnetism and Magnetostratigraphy of the Middle Triassic in the Iberian Ranges (Central Spain). In A. Morris & D. R. Tarling (Eds.), *Palaeomagnetism and Tectonics of the Mediterranean Region* (Vol. 105, pp. 59-82). London, UK: Geological Society of London Special Publications.

Rijal, M. L., Porsch, K., Appel, E., & Kappler, A. (2012). Magnetic signature of hydrocarbon-contaminated soils and sediments at the former oil field Hänigsen, Germany. *Studia Geophysica Et Geodaetica, 56*(3), 889-908. doi:10.1007/s11200-010-0040-8

Robion, P., David, C., Dautriat, J., Colombier, J.-C., Zinsmeister, L., & Collin, P.-Y. (2014). Pore fabric geometry inferred from magnetic and acoustic anisotropies in rocks with various mineralogy, permeability and porosity. *Tectonophysics, 629*, 109-122.

Salazar, J. S., Perez, L., de Abril, O., Phuoc, L. T., Ihiawakrim, D., Vazquez, M., . . . Pourroy, G. (2011). Magnetic iron oxide nanoparticles in 10−40 nm range: Composition in terms of magnetite/maghemite ratio and effect on the magnetic properties. *Chemistry of Materials, 23*(6), 1379-1386. doi:10.1021/cm103188a

Sato, M., & Ishii, Y. (1989). Simple and approximate expressions of demagnetizing factors of uniformly magnetized rectangular rod and cylinder. *Journal of Applied Physics, 66*(2), 983-985.

Sinan, S., Glover, P. W. J., & Lorinczi, P. (2020). Modelling the impact of anisotropy on hydrocarbon production in heterogeneous reservoirs. *Transport in Porous Media, 133*(3), 413-436. doi:10.1007/s11242-020-01430-z

Smolensky, E. D., Park, H. Y., Zhou, Y., Rolla, G. A., Marjanska, M., Botta, M., & Pierre, V. C. (2013). Scaling Laws at the Nano Size: The Effect of Particle Size and Shape on the Magnetism and Relaxivity of Iron Oxide Nanoparticle Contrast Agents. *J Mater Chem B, 1*(22), 2818-2828. doi:10.1039/C3TB00369H

Söffge, F., & Schmidbauer, E. (1981). AC susceptibility and static magnetic properties of an Fe_3O_4 ferrofluid. *Journal of Magnetism and Magnetic Materials, 24*, 54-66.

Stephenson, A. (1971). Single domain grain distributions: 1. A method for the determination of single domain grain distributions. *Physics of the Earth and Planetary Interiors, 4*, 353-360.

Storesletten, L. (1998). Effects of anisotropy on convective flow through porous media. In D. B. Ingham & I. Pop (Eds.), *Transport Penomena in Porous Media* (pp. 261-283). Oxford, UK: Pergamon (Elsevier).

Tarling, D. H., & Hrouda, F. (1993). *The magnetic anisotropy of rocks*. London, UK: Chapman and Hall.

Trukhan, S. N., Martyanov, O. N., & Yudanov, V. F. (2011). Stepwise magnetization of dispersed ferromagnets due to magnetic interparticle interactions. *Physics of the Solid State, 50*(3), 456-462. doi:10.1134/s1063783408030104

Turner, P., Turner, A., Ramos, A., & Sopeña, A. (1989). Palaeomagnetism of Permo-Triassic rocks in the Iberian Cordillera, Spain: acquisition of secondary and characteristic remanence. *Journal of the Geological Society, London, 146*, 61-76.

Upadhyay, S., Parekh, K., & Pandey, B. (2016). Influence of crystallite size on the magnetic properties of Fe_3O_4 nanoparticles. *Journal of Alloys and Compounds, 678*, 478-485. doi:10.1016/j.jallcom.2016.03.279

van Velzen, A. J., & Zijderveld, J. D. A. (1995). Effects of weathering on single-domain magnetite in Early Pliocene marine marls. *Geophysical Journal International, 121*, 267-278.

Wang, C., Huang, Z., Lu, Y., Tang, G., & Li, H. (2019). Influences of reservoir heterogeneity and anisotropy on CO_2 sequestration and heat extraction for CO_2-based enhanced geothermal system. *Journal of Thermal Science, 28*(2), 319-325. doi:10.1007/s11630-019-1064-1

Willems, C. J. L., Nick, H. M., Donselaar, M. E., Weltje, G. J., & Bruhn, D. F. (2017). On the connectivity anisotropy in fluvial Hot Sedimentary Aquifers and its influence on geothermal doublet performance. *Geothermics, 65*, 222-233. doi:10.1016/j.geothermics.2016.10.002

Worm, H.-U. (1998). On the superparamagnetic - stable single domain transition for magnetite, and frequency dependence of susceptibility. *Geophysical Journal International, 133*, 201-206.

Xie, J., Peng, S., Brower, N., Pourmand, N., Wang, S. X., & Sun, S. (2006). One-pot synthesis of monodisperse iron oxide nanoparticles for potential biomedical applications. *Pure and Applied Chemistry, 78*(5), 1003-1014. doi:10.1351/pac200678051003

Zhou, Y., Pugnetti, M., Foubert, A., Lanari, P., Neururer, C., & Biedermann, A. R. (in review). Quantitative comparison of 3D pore shape and distribution with magnetic pore fabrics – testing the ability of magnetic methods to predict pore fabrics in rocks.

Figure captions

Figure 1*: (a) Simplified sketches of remanence, coercivity and susceptibility variation with particle size; (b) SP-SSD threshold size as a function of measurement frequency. For the susceptibility variation, Stephenson (1971), Dearing et al. (1996) and Eyre (1997) assumed a single particle size, while Worm (1998) and Hrouda (2011) reported the behaviour for size distributions.*

Figure 2*: Comparison of measured magnetite nanoparticle properties as a function of grain size, and comparison with bulk magnetic properties. Two connected data points are shown for measurements by Lee et al. (2015), who measured clusters of particles, where particle size and cluster size were varied simultaneously. The two points correspond to the particle size (lower size value) and cluster size, respectively.*

Figure 3*: (a) Schematic sketch of synthetic sample geometry, and expected MPF anisotropy for the synthetic samples filled with different fluids at concentrations 1:5, 1:10, and 1:20. Note that the MPF anisotropy degree reflects a combination of void geometry and ferrofluid intrinsic properties. (b) Preparation of natural samples, cf J. Parés et al. (2016) for details. The samples were stored in their plastic holders and refrigerated between initial measurements and repeat measurements. (c) Thin section photograph under plane-polarized light of a mica grain from the studied red silty sandstones. Arrows depict cleavage parallel to the (001) basal plane in the grains. Visible cleavage planes have an (apparent) thickness less than 5 µm, orders of magnitude larger than the size of the magnetic nanoparticles of the ferrofluid. As far as the MPFs in the Triassic redbeds, J. Parés et al. (2016) concluded that ferrofluid within the mica cleavage planes would simply enhance the AMS ellipsoid of the sediments, due to the magnetic nanoparticles infilling such planes.*

Figure 4*: Time-dependence of AC and DC susceptibility, ratio of measured to expected susceptibility, and frequency-dependence of susceptibility for samples impregnated with EMG304 (a-c), EMG705 (d-f), EMG901 (g-i) and EMG909 (k-m). Horizontal dashed lines indicate the ideal case of equal measured and expected susceptibility (b, e, h, l), and frequency-independent susceptibility (c, f, I, m). Vertical dotted lines indicate the 3-month-period after which particles in water-based ferrofluid are expected to aggregate according to the manufacturer (a-f). Open symbols reflect repeat samples made from a different batch of EMG304 ferrofluid (a-c).*

Figure 5*: Anisotropy of AC susceptibility and its time-dependence for samples impregnated with EMG304 (a-c), EMG705 (d-f), EMG901 (g-i), and EMG909 (k-m). The rotationally prolate symmetry of the samples defines an anisotropy where $k_z > k_x = k_y$, and expected anisotropies for the different concentrations are indicated with horizontal dashed lines. The horizontal dotted line separates the fields with $k_z >$ average of k_x and k_y, and $k_z <$ average of k_x and k_y. Open symbols refer to repeat samples. The vertical dashed line indicates the critical 3-month age after which water-based ferrofluids may change properties according to the manufacturer (a-f).*

Figure 6*: Hysteresis loops, initial susceptibility, and remanence curves samples impregnated with EMG304 (a-c), EMG705 (d-f), EMG901 (g-i), and EMG909 (k-m) at concentration 1:5, and their evolution with time. All measurements shown here indicate properties parallel to x. Grey arrows show the general changes with increasing age of the sample.*

Figure 7*: Examples of AMS and MPF fabric orientation (a), MPF anisotropy degree (b) and shape (c), and mean susceptibility (d) for initial measurement, and repeat measurements after 4 years. Susceptibility and AMS parameters are given as mean of specific sites, and error bars indicate standard deviations for the site means. Dashed lines in (b) and (c) indicate equal anisotropy parameters.*

Figure 8: *Overview of changes identified in synthetic samples, and analogy drawn to rock samples. Particle aggregation and sedimentation leads to discrepancies between the void shape and the shape of the volume filled with particles. In addition, interactions between aggregated particles influence magnetic properties. Both processes affect the measured MPF*

Figure 9*: Interpretation of changes in magnetic properties of water- and oil-based fluids over time.*

(a) Variation of magnetic properties with particle size

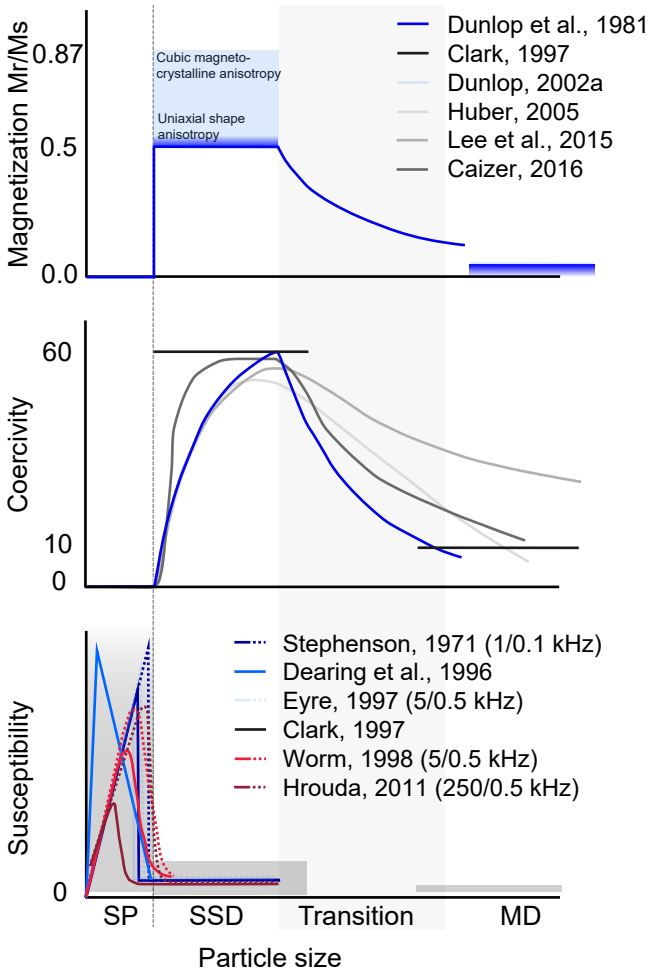

(b) Variation of SP - SSD threshold with frequency

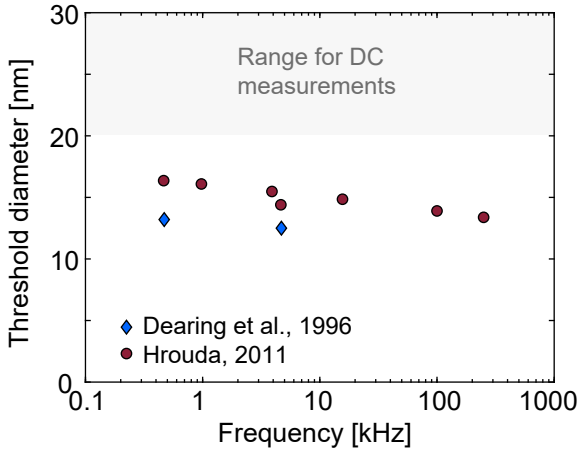

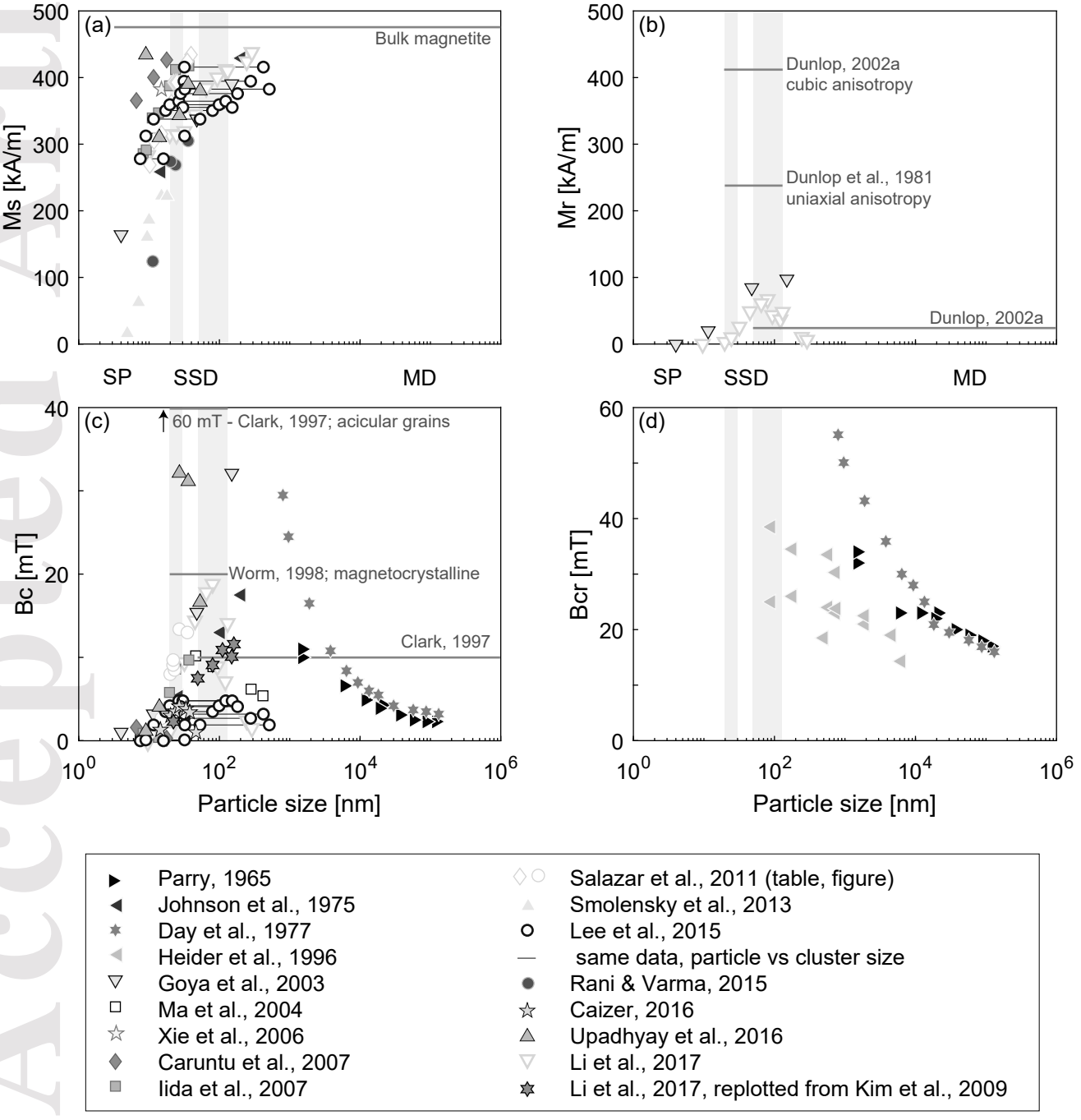

(a) Synthetic samples and expected MPF properties

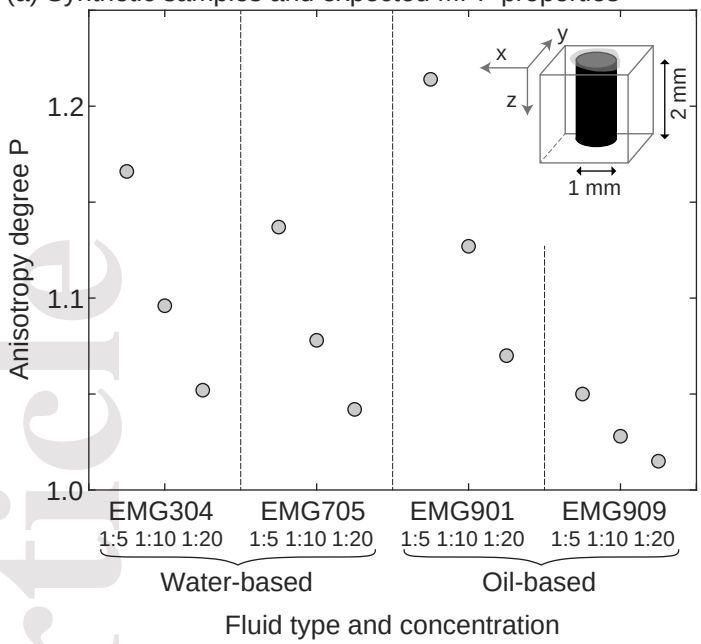

(b) Natural red sandstone samples: Preparation

(c) Natural red sandstone samples: Thin section image